PCCP

Cite this: *Phys. Chem. Chem. Phys.*, 2011, **13**, 14119–14130

www.rsc.org/pccp

PAPER

Temperature-dependent intensity anomalies in amino acid esters: weak hydrogen bonds in protected glycine, alanine and valine†

Katharina E. Otto,[a] Susanne Hesse,[a] Tobias N. Wassermann,‡[a] Corey A. Rice,§[a] Martin A. Suhm,*[a] Thorsten Stafforst¶[b] and Ulf Diederichsen[b]

Received 23rd March 2011, Accepted 8th June 2011
DOI: 10.1039/c1cp20883g

Esters of glycine, alanine and valine are investigated by FTIR and Raman spectroscopy in supersonic jets as gas phase model systems for the neutral peptide N-terminus. The NH-stretching vibrations exhibit very large temperature- and substitution-dependent intensity anomalies which are related to weak, bifurcated intramolecular hydrogen bonds to the carbonyl group. Comparison to theory is only satisfactory at low temperature. Spectral NH aggregation shifts are small or even negligible and the associated IR intensity is remarkably low. In the case of valine, chirality recognition effects are nevertheless detected and rationalized. Comparison to quantum-chemical calculations for dimers shows that dispersion interactions are essential. It also rules out cooperative hydrogen bond topologies and points at deficiencies in standard harmonic treatments with the linear dipole approximation.

1 Introduction

Amino acids offer a wide range of intra- and intermolecular interactions, which change with the aggregation stage, charge, side chain and peptide incorporation.[1] They have been extensively studied in the gas phase,[2,3] in supersonic jets,[4–6] in matrix isolation[7–11] and in polar environments.[12,13] Here, we block the acidic OH group by esterification.[14] What remains is a weak intramolecular interaction between the NH_2 group and the carbonyl group, which may be replaced by intermolecular variants as well as NH···NH contacts upon aggregation. In contrast to unprotected amino acids,[15] zwitterion formation[16] is suppressed even in a polar environment.

The conformational freedom is illustrated in Fig. 1. Rotation around the first torsional angle (nitrogen lone pair–N–C–C, in the following abbreviated as NC) directly modulates the interaction between the N–H bonds and the electron density at the carbonyl group. Rotation around the second torsional angle (N–C–C–O, abbreviated as CC) is most feasible and allows for a switch from carbonyl to ester oxygen coordination. Torsion around the ester bond (C–C–O–C) is rather stiff, partially mimicking the amide bond, whereas torsion around the third dihedral angle shown (C–O–C–C, abbreviated as OC) should be considered if one goes beyond the methyl ester. By using *t* for torsional angles of 180° ± 30° (*g* for 60° ± 30° and *c* for 0° ± 30°), the conformation shown in Fig. 1 is denoted *ttt* for the first, second and third torsional angles in this sequence.

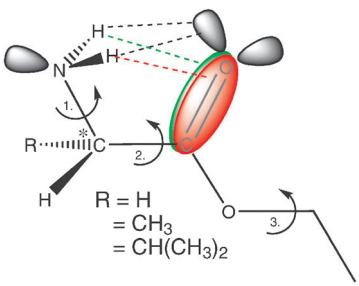

Fig. 1 Scheme for the nomenclature of the different conformers of the examined amino acid esters. The 1st (NC), 2nd (CC) and 3rd (OC) dihedral angles are used, yielding *ttt* in this case.

The interplay between intra- and intermolecular contacts is normally best probed in the N–H stretching fundamental range,[14] but the very low IR intensity of uncoordinated pyramidal NH_2 group vibrations and the oscillator coupling between the two geminal N–H bonds present additional challenges. The former can be met by the inclusion of Raman spectroscopy, whereas the latter was avoided chemically in an earlier study of proline esters.[17] The key result of that study was a weak aggregation signature in the IR. In proline ester dimers, a slight preference for mutual N–H···O=C

[a] *Institut für Physikalische Chemie, Universität Göttingen, Tammannstr. 6, D-37077 Göttingen, Germany. E-mail: msuhm@gwdg.de*
[b] *Institut für Organische und Biomolekulare Chemie, Universität Göttingen, Tammannstr. 2, D-37077 Göttingen, Germany*
† Electronic supplementary information (ESI) available. See DOI: 10.1039/c1cp20883g
‡ Present address: Laboratoire de Chimie Physique Moléculaire, École Polytechnique Fédérale de Lausanne, CH-1015 Lausanne, Switzerland.
§ Present address: Department of Chemistry, University of Basel, CH-4056 Basel, Switzerland.
¶ Present address: Interfacultary Institute of Biochemistry, University of Tuebingen, D-72076 Tuebingen, Germany.

coordination leading to a folded ring involving 8 heavy atoms was predicted. Hydrogen bond-induced aliphatic N–H stretching fundamental shifts in dimers were found to be small, in rather pronounced contrast to aromatic N–H stretching modes.[17]

The purpose of the present contribution is to explore this weak vibrational signature of NH_2 hydrogen bonding for ethyl esters of the elementary amino acids glycine, alanine and valine. Ethyl esters are preferred over methyl esters because of their increased stability with respect to polymerization. For the study of neutral aliphatic amino acids and their esters, detection techniques based on UV-absorption like (two-photon) ionization or laser-induced fluorescence,[18] IR-UV double resonance techniques[19,20] or other mass spectrometric action-spectroscopy[16,21,22] are less feasible. Instead, for the elementary model systems studied here, direct FTIR absorption spectroscopy and spontaneous Raman scattering appear to be the most suitable vibrational techniques available.[17,23] As will be demonstrated, there are remarkable and fairly systematic temperature-dependent intensity effects, combined with the phenomenon of non-shifting hydrogen bonds and with subtle chirality recognition. Raman jet spectroscopy turns out to be crucial in uncovering these phenomena, as is the consideration of dispersion effects in the interaction. The results are of relevance for the potential role of N-terminal amino acids in peptide recognition and catalysis under non-protonated conditions. Such conditions may exist in solution, with typical pK_a values of the (protonated) amino group between 7 and 8 and sometimes as low as 6.[24] However, solution studies of the NH stretching dynamics are strongly affected by the intense OH stretching band of the water solvent. Therefore, the present gas phase spectra offer new insights into the properties of this functional group. Our spectra also provide new test cases for the various theories on red-, blue- and non-shifting hydrogen bonds.[25,26]

2 Methods

Due to their instability regarding polymerization, the amino acid esters were always freshly prepared from their hydrochlorides (glycine ethyl ester hydrochloride, 99%, ABCR; L-alanine ethyl ester hydrochloride, 99%, Aldrich; L-valine ethyl ester hydrochloride, 99%, Acros Organics; DL-valine ethyl ester hydrochloride, 99%, ABCR). The hydrochlorides were dissolved in water, cooled to 0 °C and $\geq$ 1 equivalent of aqueous K_2CO_3 (Grüssing GmbH, 99.5%) was added. The mixture was stirred at 0 °C for five minutes and brought to room temperature. After another five minutes of stirring the solution was extracted with dichloromethane (Roth, $\geq$ 99%), dried over Na_2SO_4 (ABCR, 99%), and the solvent was evaporated under reduced pressure. The esters were obtained as colourless oil with overall yields of $\geq$ 90% and their purity was checked by NMR spectroscopy (for detailed information see ESI†).

FTIR spectra at 2 cm^{-1} resolution were recorded in a pulsed slit jet expansion.[17] The jet chamber was crossed by a mildly focussed and recollimated Bruker IFS 66v/S probe beam over a total length of 0.78 m. Either the equilibrated gas phase or a supersonic jet expansion emerging from a 0.6 m slit nozzle with a slit width of 0.2 mm was probed close to the nozzle over a varying cross section, which averages around 15 mm × 15 mm. The compounds were highly diluted in a carrier gas (99.996% He, Linde). The concentration was adjusted by letting the rare gas flow through a thermostated saturator filled with the liquid esters. Variations in concentration could be obtained by setting the saturator to different temperatures. For details, see ref. 27 and the ESI.† The reported approximate gas phase concentrations are based on comparison with quantum chemical intensity calculations in the IR carbonyl stretching region on the MP2/6–311 + G* level of approximation.

Spontaneous Raman scattering measurements[28] were carried out using similar gas mixtures of the amino acid esters in He. They were expanded *via* a 4 × 0.15 mm^2 slit nozzle, pumped by a 500 m^3 h^{-1} Roots pump. The beam of a frequency doubled cw $NdYVO_4$-Laser (Coherent Verdi V18, 18 W, λ = 532 nm) was focused onto the expansion at distances from the nozzle exit of 1 and 3 mm. Variation of the nozzle distance can lead to relaxation effects by collisions of the molecules with the carrier gas atoms.[29,30] Substance concentrations were adopted from the IR experiment. At 90° angle, the scattered light was collected and collimated using a fast camera lens (Nikon, ∅ = 50 mm, *f*/1.2). It was then focused onto the entrance slit of the monochromator (McPherson Model 2051 *f*/8.6, *f* = 1000 mm) using an achromatic planoconvex lens (Edmund Optics, ∅ = 50 mm, *f*/7). A Raman edge filter (L.O.T., ∅ = 25 mm, OD 6.0, T > 90%, 535.4–1200 nm) was used to eliminate Rayleigh scattered photons before the dispersion by the monochromator. A liquid N_2 cooled back-illuminated CCD camera (PI Acton, Spec-10: 400 B/LN, 1340 × 400 pixel) served as the detection device. The primary wavelength calibration of the spectra was carried out using the lines of a Ne I emission light source. Cosmic ray signals were removed by the comparison of block-averaged spectra.

Quantum chemical calculations (structure optimizations and harmonic frequency calculations) were explored for these systems using the Gaussian09[31] package. The computational methods include B3LYP/6-311++G** (abbreviated B3LYP), B97D/TZVP/TZVPFit (abbreviated B97D), MP2/6-311 + G* (MP2) and MP2/aug-cc-pVTZ (MP2/aug). For some MP2 levels, Raman intensities were not available but rather adopted from the smaller basis set MP2 prediction or, for the dimers, from B97D predictions. At levels where zero-point energy corrections were not available because of the involved computational effort beyond that of the structure optimization, these were adopted from a lower level, as indicated in the corresponding tables and figures.

3 Results and discussion

The results are organized according to increasing complexity of the amino acid, always comparing the experimental spectra with quantum chemical spectral predictions.

3.1 Glycine

The most stable structure of glycine ethyl ester (*ttt*) is shown in Fig. 2, together with three higher-lying conformations. Torsion of the ester group into a gauche position (*ttg*) comes with a small energy penalty but this is not expected to lead to separate spectroscopic features in the investigated range.

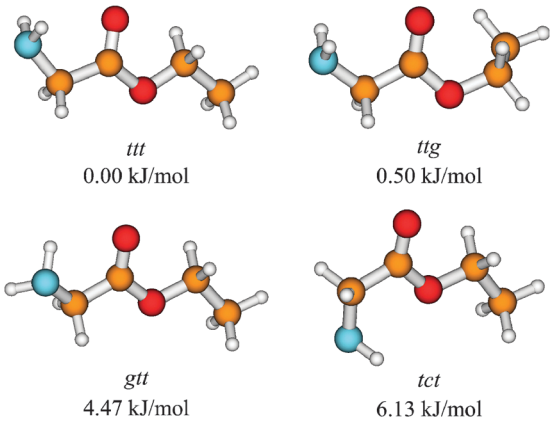

Fig. 2 The most stable structures obtained at the MP2/aug-cc-pVTZ level of approximation for monomeric glycine ethyl ester along with their relative energies including zero-point energy (ΔE_0).

The amino group clearly prefers a symmetric double coordination of the carbonyl group by both N–H bonds.[32,33] We note that this is the same arrangement as in neutral gas phase glycine itself, according to high level quantum chemical calculations,[1,34,35] microwave structures[36] and Raman spectroscopy.[6] In contrast, N-terminal glycine in a peptide can also form a N–H···NH_2 hydrogen bond[37] if the first peptidic NH-group is available. Coordination of the carbonyl group by only one N–H (*gtt*) or coordination of the ester oxygen (*tct*) are both associated with an energy penalty of more than 4 kJ mol^{-1} and should normally not be observed in a supersonic jet, except very close to the nozzle.[6] One may speculate that the double coordination in *ttt* and *ttg* profits from overlap with the π-orbital of the carbonyl group, in the presence of an unfavorable angle for interaction with the oxygen lone pair (see Fig. 1).

In the N–H stretching region of isolated glycine ethyl ester, one thus expects two stretching bands due to symmetric and antisymmetric motion of the two geminal bonds. For an unsubstituted amine such as methylamine, they fall in the range of 3360–3424 cm^{-1} and are separated by ~64 cm^{-1} [38–41] with the lower band corresponding to symmetric stretching motion. This pattern is reproduced reasonably well by a range of harmonic quantum chemical calculations (see Table S1 in the ESI†). The splitting is exaggerated (78 cm^{-1} at the B3LYP level, 90–100 cm^{-1} at B97D and MP2 levels). Nevertheless, such calculations allow for a relative prediction of the glycine ethyl ester spectra. Here, the symmetric/antisymmetric splitting is predicted consistently smaller by about 8 ± 2 cm^{-1}, whereas the position of the symmetric stretch is always within 10 cm^{-1} of the methylamine value. Harmonic quantum chemical calculations (see Table S2, ESI†) consistently indicate that the antisymmetric mode of the glycine ethyl ester has about 3–5 times more IR intensity than the symmetric one, whereas the Raman intensity is higher by a factor of 2–3 in the symmetric case.

The experimental spectra recorded in the gas phase at room temperature fully confirm the predicted NH band positions but provide a rather different picture in terms of intensity and number of bands (Fig. 3). The IR spectrum (trace (a)) contains three weak bands of more or less similar intensity, whereas the Raman spectrum (trace (d)) only shows the lowest of these

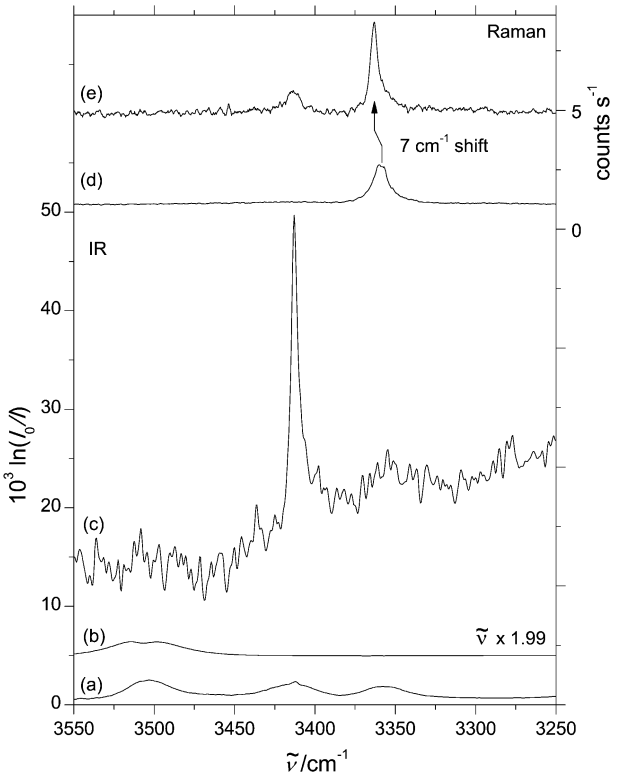

Fig. 3 Experimental FTIR and Raman spectra of glycine ethyl ester in He in the NH-stretching region: (a) gas phase (IR), 170 mbar, 0.03% glycine ethyl ester; (b) C=O stretching fundamental on a 1.99 × stretched wavenumber scale after 100-fold intensity compression; (c) jet (IR) scaled by a factor of 100 to match the CH-region of the gas phase spectrum, 0.03%, 0.7 bar stagnation pressure; (d) gas phase (Raman), 0.2 bar, 0.01%; (e) jet (Raman) scaled by a factor of 14 to match the CH-region of the gas phase, nozzle distance 3 mm, stagnation pressure 0.8 bar, 0.01%.

bands together with a very weak trace of the second-lowest (30–100 fold weaker relative intensity). The extra band at a higher wavenumber in the IR spectrum can be explained as in the case of proline esters.[17] It is due to the weak overtone of the carbonyl stretching vibration, as shown in trace (b) after multiplication of the fundamental wavenumber by 1.99. This illustrates how weak the N-terminal NH stretching bands are in the IR, sometimes even preventing their identification.[3] The symmetric NH-stretching mode would be expected at 3360 ± 10 cm^{-1} and indeed it is observed at 3356 cm^{-1}. The antisymmetric NH-stretching mode would be expected ~64–8 cm^{-1} higher and indeed it is found at 3413 cm^{-1}. If there were no 10–30-fold attenuation of the antisymmetric Raman band and no ~5-fold attenuation of the antisymmetric IR stretching transition compared to theoretical expectations, everything would be in perfect agreement for the gas phase spectrum at room temperature.

In a supersonic jet, the spectral intensities change drastically. The jet spectra are displayed in Fig. 3 on a scale where the integral C–H band intensity is comparable to that in the gas phase. Assuming that the C–H transitions are not very temperature- and clustering-sensitive, this indicates that the central IR band gains in intensity by a factor of 7 ± 2, whereas the other two do not and therefore disappear in the noise level.

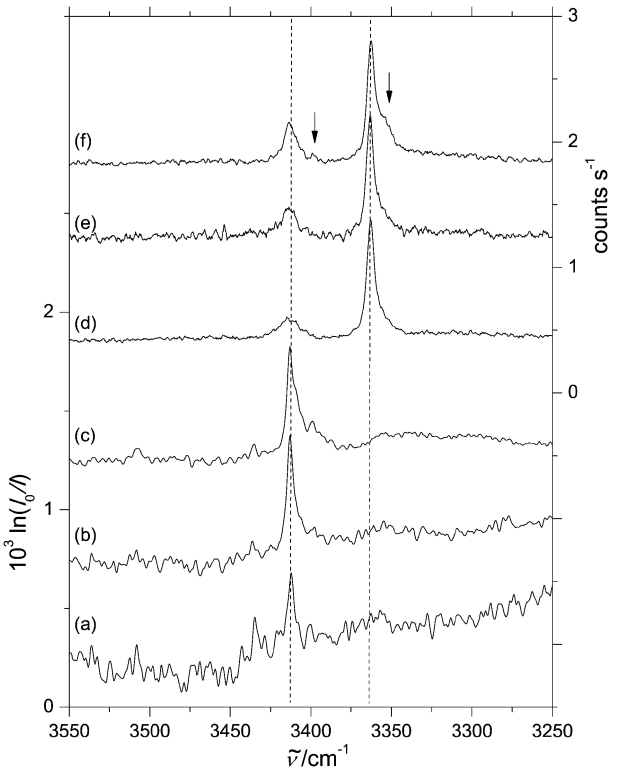

Fig. 4 Experimental FTIR and Raman spectra of glycine ethyl ester in He in the NH-stretching region with increasing concentration scaled to a similar integral band intensity of the antisymmetric NH-stretching vibration of the monomer. (a)–(c) Jet spectra (IR) measured at a stagnation pressure of 0.7 bar, (a) 0.01%, scaled by 3.6, (b) 0.03%, scaled by 1.9, (c) 0.06%; (d)–(f) jet spectra (Raman) measured at a stagnation pressure of 0.8 bar, (d) nozzle distance 1 mm, 0.01%, (e) nozzle distance 3 mm, 0.01%, scaled by 3.1, (f) nozzle distance 3 mm, 0.03%, scaled by 1.9.

In the Raman spectrum, the central band gains by a factor of 25 ± 5, whereas the lowest frequency band increases by less than a factor of 2 and shifts somewhat to a higher wavenumber. Detailed values may be found in Table S3 (ESI†).

As a consequence, jet cooling changes the intensity ratio of the central band to the low-wavenumber band from 1 to more than 5 in the IR and from 0.02 ± 0.01 to 0.3 ± 0.1 in the Raman case. To explain this temperature effect, one might invoke cluster formation in the jet combined with a negligible clustering shift. While small frequency shifts are rare in hydrogen bonding, they are conceivable, given the existence of both red- and blue-shifted hydride stretching vibrations.[25,26] Therefore, Fig. 4 shows sequences of jet expansions, with clustering conditions increasing from bottom to top within a given method. There are indeed weak cluster features to lower wavenumbers (marked with arrows), but the main peaks do not change substantially, thus ruling out a major intensity distortion by cluster formation. This is confirmed by the scaling factors chosen to keep the monomer signal intensity more or less constant. They are approximately inversely proportional to concentration, as expected. Minor cluster contributions on top of the IR monomer bands should however not be ruled out and are highly probable. Independent of the nature of the intermolecular hydrogen bonds in these clusters (N–H···O=C or N–H···O–C or N–H···N–H), it is remarkable that the red-shifts do not exceed 15 cm^{-1}. The cluster-induced red-shift of the carbonyl stretching fundamental (10–15 cm^{-1}) is of comparable size and the blue-shift of the ester C–O stretching mode is as large as 14 cm^{-1}, both supporting a N–H···O=C interpretation (see Fig. S1, ESI†). We note that the NH bending mode gives rise to a single monomer band that is split into red- and blue-shifted bands in the clusters, also indicative of intermolecular N–H···O=C hydrogen bonds. Further details may be found in the ESI† (Fig. S1 and Table S4).

The monomer interpretation of the peaks observed in the jet spectra is further supported by quantum chemical calculations. Table S2 (ESI†) shows that the theoretical intensity predictions are matched quite well by the experimental jet spectra, whereas the room temperature gas phase spectra strongly disagree with theory. Evidently, the effect must be related to the effective temperature of the amino acid esters, with lower temperatures promoting the asymmetric stretching intensity. It is noteworthy that a He droplet experiment for glycine[42] also revealed a dominance of the antisymmetric NH stretch, which in this case occurs at 3436 cm^{-1}.

We emphasize that microwave studies of the methyl ester of glycine[33] at room temperature have identified the most stable bifurcated hydrogen bond structure (*ttt*), but also significant population of a CC torsional state, the fundamental excitation of which was estimated at 40–70 cm^{-1}, along with at least 7 other populated states. This underscores the floppiness of the molecule at room temperature and our work suggests that some of these excited states have a much weaker antisymmetric NH stretching mode than the ground state. Indeed, a rough estimate of the vibrational ground state population of glycine ethyl ester at room temperature is 0.3%, which may rise to >30% in the jet expansions.

If we attribute the jet cooling effects to the strengthening of the bifurcated NH_2···O=C hydrogen bond, this particular interaction has remarkable properties. It leads to a small but distinct blue-shift of the symmetric NH-stretch and an enormous intensification of the antisymmetric stretching mode both in Raman (×25) and IR (×7) spectra.

To corroborate the origin of the intensity anomaly in glycine ethyl ester, we have carried out corresponding experiments with 2-methoxyethylamine,[43] which lacks the carbonyl group. As elaborated in the ESI†, there is an analogous pattern of symmetric and antisymmetric NH-stretching vibrations (Fig. S2, ESI†). The splitting is closer to the methylamine case (Table S1, ESI†), fully in line with theoretical predictions, and there is a contribution from a secondary isomer. Most importantly, the s/as intensity ratio in the Raman spectrum is now independent of temperature within experimental error bars (Table S5, ESI†). Absolute Raman intensities change at most by a factor of 2 in the jet, as opposed to 25 ± 5 in the case of the glycine ester. Furthermore, there is no blue-shift of the symmetric NH-stretching mode upon cooling. From this control experiment, it follows that the NH_2 intensity and shift anomalies are correlated with the presence of a carbonyl group in the α position.

One may now speculate that the intensity of the anti-symmetric stretching mode is promoted by the interaction

with the π-orbital, where the stretching N–H bond may profit from the polarization of the lobe pointing in its direction, while the contracting N–H bond recedes from the other lobe. In order to test this, we also compare IR and Raman intensities of methylamine at the same levels of approximation in Table S2 (ESI†). The non-systematic behaviour of the IR and Raman intensities, also across different computational levels, suggests that this is not the case. Following the formal IR and Raman signal strengths along the NC and CC torsional angles (see Fig. S3–S6 in the ESI†) does not provide further insights into the observed intensity effects, either. In contrast, these relaxed scans would indicate that the IR intensities of methoxyethylamine are more sensitive to thermal excitation than those of glycine ethyl ester. Either the employed electronic structure approach (MP2/6–311+G*) is unable to describe the intensity trends or an anharmonic treatment of the torsional states is needed.

3.2 Glycine ester aggregates

Different hydrogen-bonded dimer topologies were explored for the ethyl ester of glycine. Their nomenclature involves the size of the hydrogen-bonded ring (counting only heavy atoms). Two isolated N–H hydrogen bonds lead to 8-rings and can either engage carbonyl oxygen (c) or ester oxygen atoms (e). A cooperative N–H···N–H···O arrangement involves 5 heavy atoms including either a carbonyl (c) or an ester (e) oxygen. This gives rise to 5 different topologies (8^{cc}, 8^{ee}, 8^{ec}, 5^{c}, 5^{e}), of which the first four are exemplified in Fig. 5. Topology 5^{e} was discarded because of its high energy. When dispersion interaction is included, all four structures are predicted to be rather compact. This has major consequences for the predicted energy sequence, which is shown in Fig. 6 (including harmonic zero point energy). Cooperative 5-ring structures stop to be relevant when dispersion interaction is included. All methods

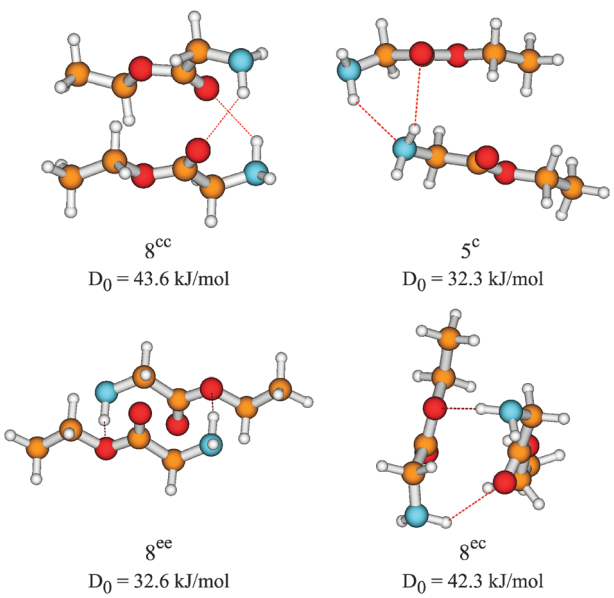

Fig. 5 Different dimer structures of glycine ethyl ester optimized on the MP2/6-311+G* level of approximation including their zero-point-corrected dissociation energies (D_0).

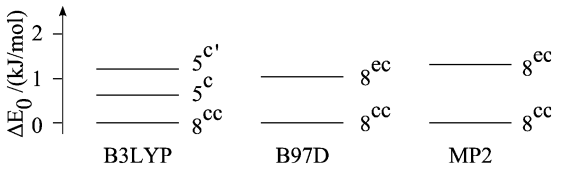

Fig. 6 Energy level scheme including zero-point energies (ΔE_0) for different dimer species of glycine ethyl ester optimized on different calculation levels.

predict 8^{cc} as the global minimum structure, closely followed by an unsymmetrical 8^{ec} topology.

Indications for the presence of different dimer structures in the jet expansions can be expected from the IR spectra. In the carbonyl stretching region with its large oscillator strength, cluster bands can be used for a semiquantitative assessment of their concentration. It is likely (and confirmed by theoretical calculations at several levels) that the average C=O IR-intensity does not change by more than a factor of two when this group engages in hydrogen bond formation. Based on this, the C=O stretching band shown in Fig. S1 (ESI†) and in the top trace of Fig. 7 indicates that around 60% of the C=O groups are present in the clustered form for a 0.06% expansion of glycine ethyl ester in He. Assuming that dimers dominate the cluster distribution, this corresponds to a dimer fraction of up to 40%. The value will be smaller if larger clusters are present as well. The fact that the cluster C=O band is red-shifted relative to the monomer band suggests the presence of intermolecular N–H···O=C hydrogen bonds which are stronger than the intramolecular ones. As a consequence, the C–O stretching transition near 1200 cm^{-1} is blue-shifted because this bond is strengthened when the adjacent C=O bond is weakened. Simulated stick spectra (lower traces of Fig. 7) allow for a narrowing down of the conformational options. At the B3LYP level, where 8^{cc} and 5^{c} are predicted to be particularly stable, both fit the experimental spectra at least qualitatively. At the B97D level this is only the case for 8^{cc}, but not for the second most stable 8^{ec} structure. At the MP2 level both 8^{cc} and 8^{ec} match the experimental shift qualitatively.

The most striking result is obtained when transferring the 40% dimer simulation to the NH stretching range recorded under identical conditions. The predicted IR dimer features are far too strong. In the simulation shown in Fig. 8 they had to be attenuated by a factor of 10 relative to the monomer. Despite this attenuation the 5^{c} prediction at the B3LYP level is still too strong and fails completely in matching experimental features. The 8^{cc} intensity prediction is also too high. Similar remarks apply to the B97D intensities. In addition, qualitatively wrong blue-shifts are predicted. The MP2 simulation is qualitatively satisfactory but the reduction of the stick length by up to a factor of 10 still needs to be explained. One possibility is an increased width of the dimer bands. Indeed, there is some indication of a broad background at a lower wavenumber relative to the monomer absorptions. However, this may also be due to larger clusters and does not apply to the more structured features near 3400 cm^{-1}. The other possibility is a drastic overestimation of the IR band strength—not unreasonable for such a weakly IR-active oscillator. However, the predicted increase of the low infrared NH

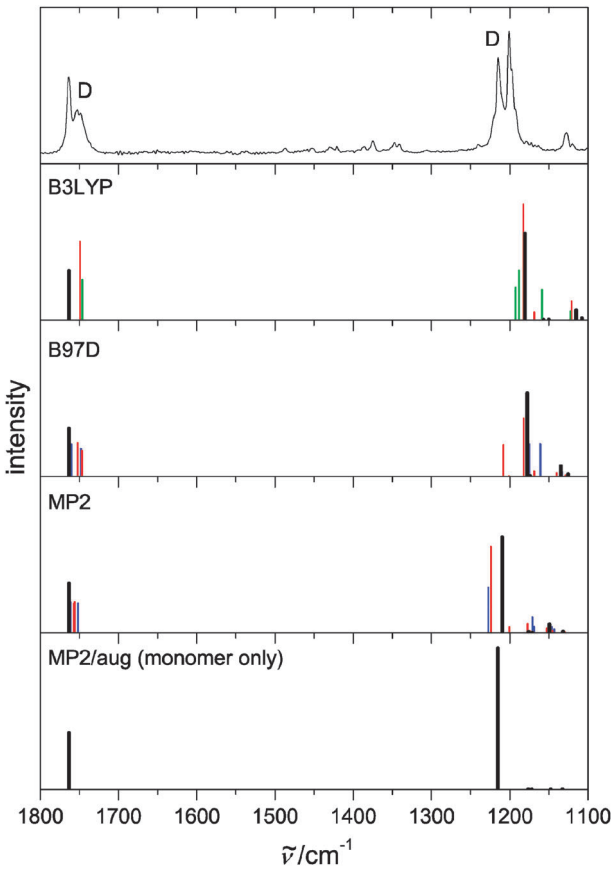

Fig. 7 Comparison of the IR jet spectrum in the carbonyl stretching and fingerprint region (0.06% glycine ethyl ester in He) to calculated spectra of the two most stable dimer structures of a given method assuming 40% dimer fraction visible in the IR spectrum. Colour code: black (thick): monomer (*ttt*), red: 8^{cc}–, blue: 8^{ec}–, green: 5^{c}–dimers. The calculated spectra are shifted such that the harmonic monomer C=O stretching fundamental matches the experiment (namely -26 cm^{-1} (B3LYP), $+26$ cm^{-1} (B97D), -29 cm^{-1} (MP2) and -16 cm^{-1} (MP2/aug)).

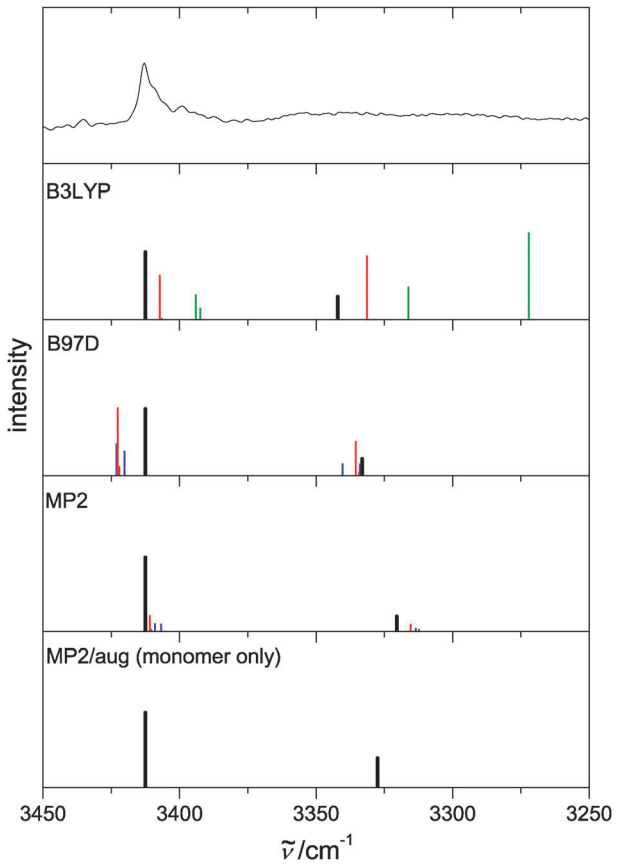

Fig. 8 Comparison of the IR jet spectrum in the NH-stretching region (0.06% glycine ethyl ester in He) to calculated spectra of the two most stable dimer structures of a given method assuming a 4% dimer fraction instead of the 40% extracted from the C=O range (see the text). This is a strong indication of either band broadening or overestimated infrared dimer NH intensities. Colour code: black (thick): monomer (*ttt*), red: 8^{cc}–, blue: 8^{ec}–, green: 5^{c}–dimers. The calculated spectra are shifted such that the harmonic monomer antisymmetric NH stretching fundamental matches the experiment (namely -167 cm^{-1} (B3LYP), -84 cm^{-1} (B97D), -238 cm^{-1} (MP2) and -202 cm^{-1} (MP2/aug)).

oscillator strength upon coordination of a C=O group is very robust. We find it in complexes of methylamine with methyl acetate (not shown) and we find it at different computational levels within the harmonic approximation.

In this situation, Raman spectroscopy aids in the analysis because it exhibits rather strong and therefore more robust N–H scattering strengths. Fig. 9 shows a dilute expansion for which one can roughly estimate a 20% dimer fraction. A more precise cluster quantification is difficult because the C=O stretching range is not very Raman active. Again, the B3LYP simulation fails completely in terms of shift and intensity. However, the B97D simulation provides quite reasonable Raman intensities. Combining them with the more reliable MP2 band positions gives a plausible representation of the experimental Raman spectra and shows that dimers do not have excessive bandwidths. Therefore, the failure of all employed methods to reproduce the IR intensity of the clusters is most likely related to an overestimation of IR band strengths by an order of magnitude. Either more accurate dipole hypersurfaces or an anharmonic treatment will be needed to explain the low intensity of these cluster IR spectra.

We conclude that glycine ethyl ester clusters can be generated in high abundance but narrow IR spectral features, attributable to dimers (most likely 8^{cc}), in the NH stretching range are unexpectedly weak. B3LYP calculations fail completely, B97D calculations predict qualitatively wrong shifts, whereas MP2 predictions of dimers are consistent with the experiment apart from IR intensities which are too high by about an order of magnitude.

3.3 Alanine

At this stage, it is advisable to switch to the homologous ester of alanine, discussing the analogies and differences in the glycine case. Based on the insights obtained, B3LYP calculations will not be considered further, and B97D predictions will only be used to borrow Raman intensities. The most stable structures of the monomer are shown in Fig. 10. The *ttt* structure is again particularly stable, consistent with an electron diffraction study of the methyl ester[44] and both experimental and theoretical evidence for the parent compound alanine.[4,45]

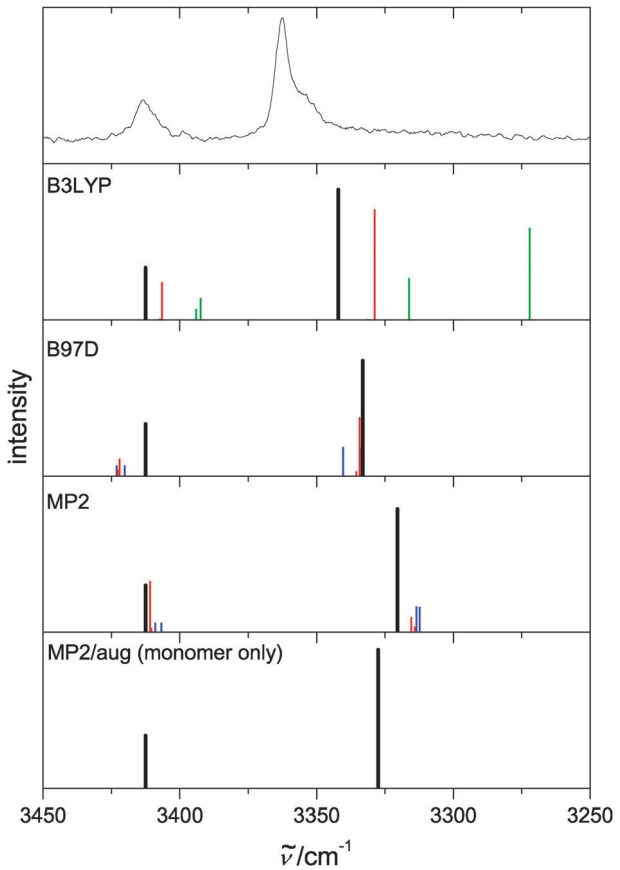

Fig. 9 Comparison of the Raman jet spectrum (0.03% glycine ethyl ester in helium, 3 mm) to calculated spectra of the two most stable dimer structures of a given method assuming a 20% dimer fraction visible in the Raman spectrum. Colour code: black (thick): monomer (*ttt*), red: 8^{cc}–, blue: 8^{ec}–, green: 5^{c}–dimers. The calculated spectra are shifted such that the harmonic monomer antisymmetric NH stretching fundamental matches the experiment.

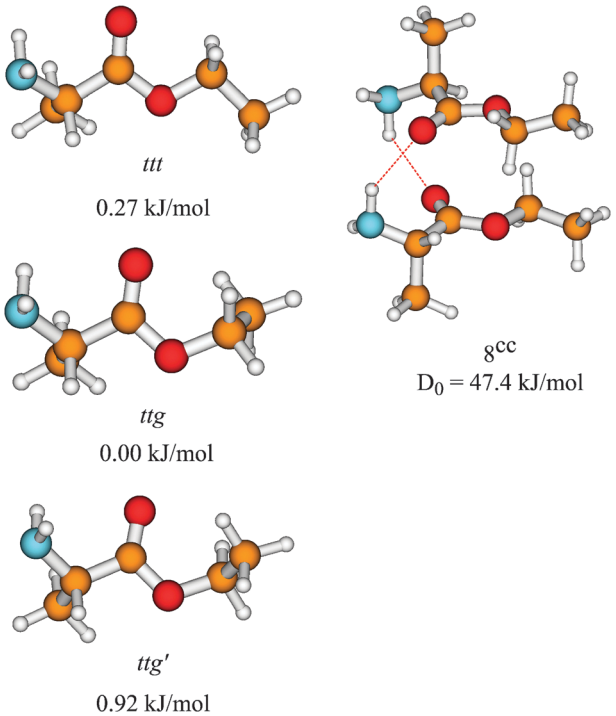

Fig. 10 The most stable structures obtained at the MP2/aug-cc-pVTZ level for the monomeric alanine ethyl ester along with their relative energies including zero-point energy (ΔE_0) at the MP2/6–311+G* level and the most stable homochiral dimer (8^{cc}) obtained at the MP2/6–311+G* level along with its zero-point corrected dissociation energy (D_0) into two *ttt* monomers.

Interestingly, the *ttg* structure with two methyl groups on the same side now competes with *ttt*, presumably due to dispersive interactions. At the highest level considered here, it is even more stable than *ttt*, but only by a small margin. In contrast, rotation of the methyl group to the other side (*ttg′*) leads to a somewhat higher energy. As discussed for glycine, this subtle isomerism is not expected to appear in low resolution spectra. Similar to the glycine case, torsion of the NH_2 group and coordination of the ester oxygen do not lead to competitive structures. However, due to the symmetry breaking of the alanine CH_3 group, the first torsional angle (Fig. 1) is now different from 180°. Depending on the level of calculation, it ranges between 175° and 178° (see Table S6, ESI†). The symmetry breaking may also be expressed in terms of the difference between the two N–H···O=C bond lengths. It amounts to 29–35 pm, which may be compared to the experimental value of 18(4) pm for the parent compound alanine.[4] A substantial fraction of the effect is due to torsion around the CC bond, which allows the ester oxygen to avoid contact with the alanine CH_3 group. This should not affect the monomer NH spectra significantly and indeed they show just the same anomalies as the glycine case, namely three bands in the gas phase IR spectrum, with the central one gaining intensity upon jet cooling and the others not (see Fig. S7, ESI†). This is consistent with the non-observation of the symmetric NH stretching mode in matrix isolation.[46] In the Raman spectra, the antisymmetric band is again very weak in the gas phase but gains intensity in the jet. Compared to glycine gain factors of ~7 (IR) and ~25 (Raman), the gains are now both around 10 (Table S7, ESI†). However, comparison to C=O stretching spectra, in which the clustering extent can be quantified (Fig. S8, ESI†), shows that the antisymmetric NH band is now directly overlapped by cluster transitions. Therefore, the monomer IR gain is actually less than 10 and one may summarize the alanine ester monomer case as being qualitatively analogous and quantitatively somewhat less pronounced than the glycine case. This is also true for the slight blue-shift of the symmetric stretching band with jet cooling. Reference spectra with racemic alanine (not shown) do not exhibit significant differences as one would expect from a monomer dominated spectrum. At this point, one can speculate about the reason for the reduced extent of the intensity anomalies upon introduction of the methyl group. Certainly, the bifurcation of the N–H···O=C hydrogen bonds in the monomer is less perfect and the overlap with the π-orbitals is reduced in favor of the lone pair interaction. Yet, the extent of the symmetry breaking is quite modest. This is also true for the decrease of the largest rotational constant in the alanine case, which might otherwise explain some change in band contour in the room temperature gas phase spectrum.

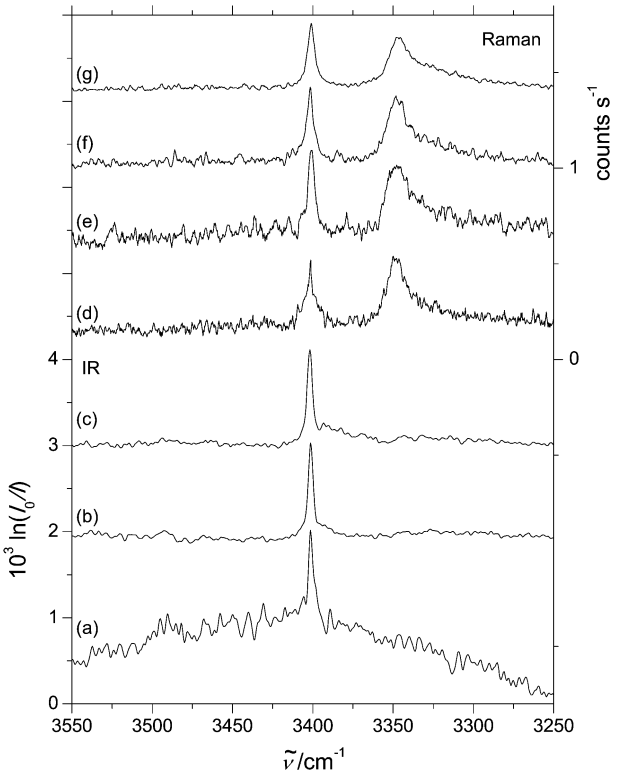

Fig. 11 Experimental FTIR and Raman spectra of alanine ethyl ester in He in the NH-stretching region with increasing concentration scaled to a similar integral band intensity of the asymmetric NH-stretching vibration of the monomer. (a)–(c) Jet spectra (IR) measured at a stagnation pressure of 0.7 bar, (a) 0.03%, scaled by 8.5, (b) 0.06%, scaled by 2.7, (c) 0.16%; (d)–(g) jet spectra (Raman) measured at a stagnation pressure of 0.8 bar, (d) nozzle distance 1 mm, 0.01%, scaled by 1.6, (e) nozzle distance 3 mm, 0.02%, scaled by 4.0, (f) nozzle distance 3 mm, 0.03%, scaled by 2.2, (g) nozzle distance 3 mm, 0.06%.

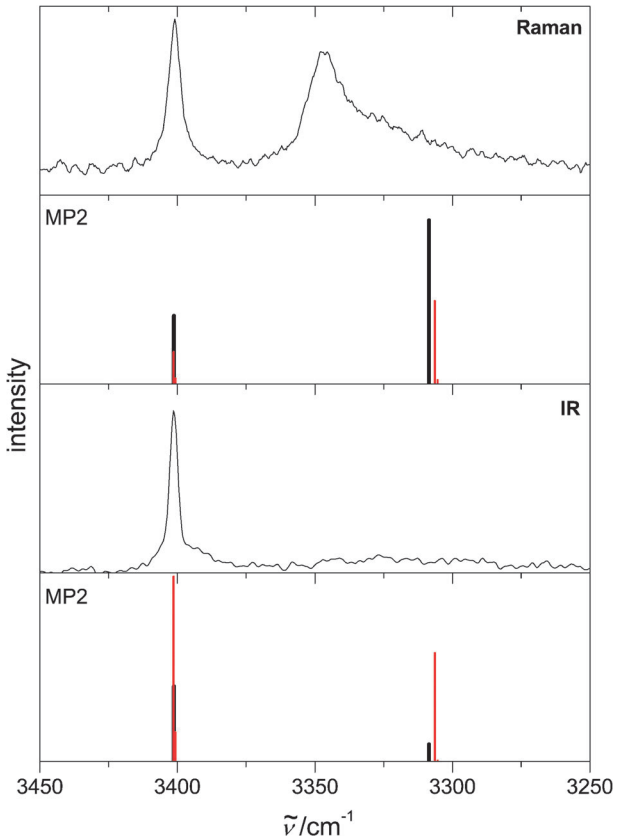

Fig. 12 Comparison of the IR jet spectrum (0.06% alanine ethyl ester in He) and the Raman jet spectrum (0.06% alanine ethyl ester in He, 3 mm) to calculated spectra of the most stable monomer (black, thick) and dimer (red) obtained at the MP2 level. The dimer fraction is set to 20% as estimated from the carbonyl stretching range. (Raman dimer intensities borrowed from B97D calculations.)

Fig. 11 shows the evolution of the alanine ethyl ester spectra with increasing cluster extent, normalized to comparable antisymmetric N–H stretching intensity. In the IR case, the cluster content can be followed in the carbonyl stretching region (Fig. S8, ESI†). It increases from about 10% in trace (a) to 20% in trace (b). Despite this strong increase, no substantial cluster absorptions are observed in the IR spectra. In the Raman case one can see some cluster contributions on the low frequency wing of the symmetric stretching band, whereas contributions in the antisymmetric stretching region appear to coincide with the monomer peak. This is supported by the spectral simulations shown in Fig. 12 for the most stable dimer of two L-alanine ethyl esters, an 8^{cc} cluster with C_2 symmetry (see Fig. 10), which has two methyl groups pointing opposite to each other. As in the glycine case, the major discrepancy is the absence of a significant symmetric NH stretching IR intensity in the experimental spectra.

3.4 Valine

The case of valine ethyl ester is again analogous in many respects but it shows three noteworthy differences. First of all, its NH stretching spectrum is complicated by conformational isomerism of the isopropyl group (Fig. 13). Its dihedral angle, which we introduce as a fourth label, can be close to 180° (*tttt*) or close to 60° (*tttg*). These valine ester structures are analogous to two out of the three lowest conformations of valine itself.[5,47] The isomerism survives the jet cooling and leads to two partially resolved doublets at 3410 and 3403 cm^{-1} for the antisymmetric (IR + Raman) and at 3353 and 3338 cm^{-1} for the symmetric (Raman) NH stretching modes (Table S8 and Fig. S9, ESI†). This is in slight contrast to the microwave evidence for one valine isomer only.[5] We note, however, some contributions from clusters, in particular, for the lower frequency peak. There is again *g*/*t* isomerism in the ester group (third label) and, depending on the level of calculation, the *ttgt* conformer is actually somewhat lower in energy than the *tttt* conformer. As this should not have spectral consequences in the NH or C=O range, it will subsequently be ignored, although the position of the ethyl group may have effects on the molecular recognition between monomers. More interestingly, the bulky isopropyl group destroys the bifurcation of the NH_2 group with respect to the carbonyl group to a significant extent (9°–19° deviation from 180° for the NC torsional angle with the larger values corresponding to higher levels, 43°–49° deviation from 180° for the CC torsional angle; Table S6, ESI†). This should be viewed together with the observation that the intensity ratio between symmetric and antisymmetric stretch is

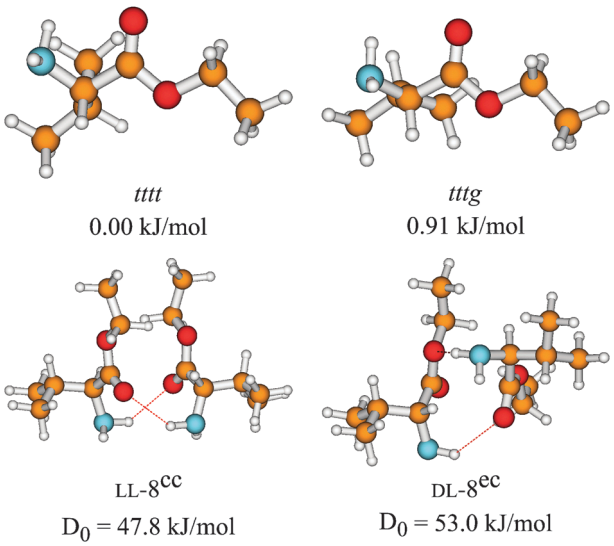

Fig. 13 The most stable structures obtained at the MP2/aug-cc-pVTZ level of approximation for monomeric valine ethyl ester. The nomenclature of the monomers includes the orientation of the isopropyl group and the relative energies including zero-point energy (ΔE_0) at the MP2/6–311 + G* level of approximation are enclosed. The hetero- (DL-8^{cc}) and homochiral (LL-8^{cc}) dimers were obtained at the MP2/6–311 + G* level and are shown along with the energy needed for their dissociation into two *tttt* monomers including zero-point energy (D_0) at the B97D/TZVP level.

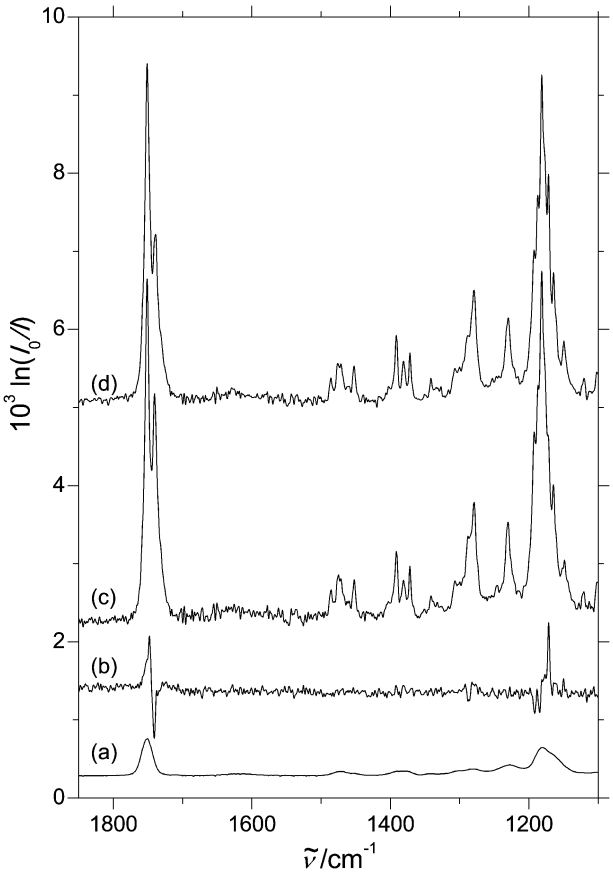

Fig. 14 Experimental FTIR spectra of valine ethyl ester in He in the carbonyl stretching and fingerprint region: (a) gas phase, 0.02%, 170 mbar, scaled by a factor of 0.1; (b) = 1.1 × (d)–(c); (c) L-valine ethyl ester in He, 0.03%, stagnation pressure 0.7 bar; (d) DL-valine ethyl ester in He, 0.03%, stagnation pressure 0.7 bar.

now essentially temperature independent (Table S8, ESI†). Instead of a factor of ~25 (glycine) or <10 (alanine), it only increases by less than a factor of 1.5 in the Raman spectrum. The IR intensity gain factor is slightly larger (3 ± 2) but rather uncertain. The symmetric NH stretch does not shift with jet cooling, also in contrast to the smaller homologues. This strongly suggests that the anomalous temperature dependence of the intensity is related to the bifurcated intramolecular hydrogen bond situation in glycine esters which is gradually lost in favor of an unsymmetric hydrogen bond pattern in alanine and particularly in valine.

The most interesting difference refers to the cluster IR signals which appear at higher concentration both in the C=O/C–O and in the N–H stretching regions. They are shown in Fig. 14 and 15, respectively. The uppermost trace corresponds to DL-valine, while the second trace refers to L-valine. The third trace shows the difference between the two, after adjusting for slight concentration differences. Where there is no chirality recognition,[48] the peaks cancel. Where homoconfigurational dimers absorb, the difference is negative because they are statistically less abundant in the racemic mixture. In regions with specific heterochiral absorption, the difference is positive.[49] One can easily see that the homochiral dimer has a stronger hydrogen bond to C=O, accompanied by a strengthening of the C–O bond. The heterochiral dimer has a lower C–O stretching wavenumber and a higher C=O stretching wavenumber, indicative of some coordination of the ester oxygen. The NH stretching range is less conclusive because of monomer/dimer overlap but also shows clear signs of chirality recognition (Fig. 15).

On the computational side, the present study is only exploratory due to the large size of the accessible conformation space. There are indeed two different particularly stable dimer topologies for LL and DL pairings. In the homochiral case an 8^{cc} dimer analogous to those for glycine and alanine is found, where the isopropyl groups point away from each other (Fig. 13). Such a structure cannot be realized easily for the DL dimer because of the associated steric hindrance. Instead, an even more stable 8^{ec} structure is found, where the isopropyl groups can also avoid each other. Although this theoretical finding has to be confirmed at higher levels of approximation and by more systematic sampling of the conformation space, it agrees nicely with the experimental observation in the C=O stretching range. Even the need to scale up the DL signals by 10–20% before subtraction fits the assumption that the racemate is more strongly bound. Possibly, the dimer observations can be extrapolated to the liquid state. A simplified simulation of the difference spectrum based on a single heteroconfigured and a single homoconfigured dimer is shown in Fig. 16. It recovers the basic spectral features and therefore supports the interpretation that two enantiomeric valine ester molecules prefer a different hydrogen bond topology than a pair of equal molecules.

3.5 Amino acid trends

Key to this work and the understanding of the observed phenomena is the series of glycine, L-alanine, L-valine, DL-valine,

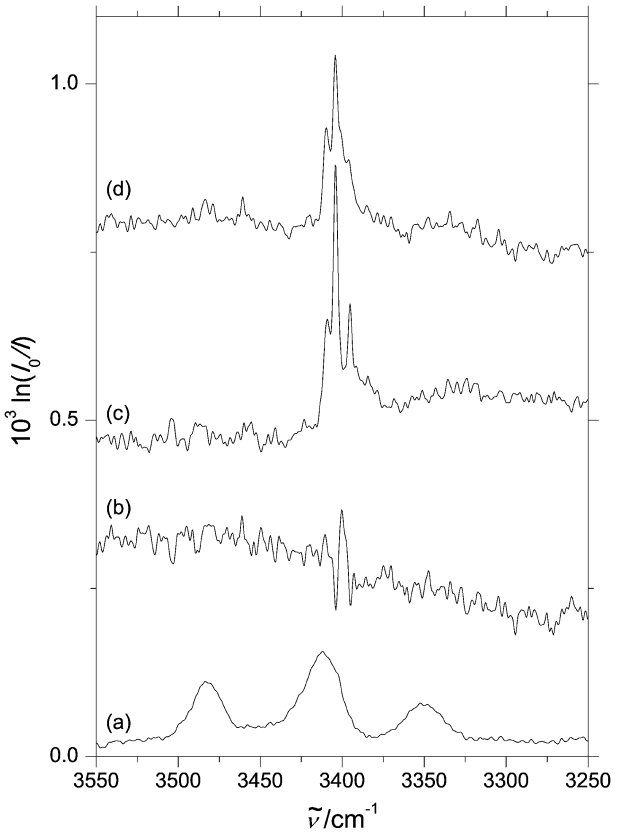

Fig. 15 Experimental FTIR spectra of valine ethyl ester in He in the NH-stretching region: (a) gas phase, 0.02%, 170 mbar, scaled by a factor of 0.1; (b) = 1.2 × (d)–(c); (c) L-valine ethyl ester in He, 0.03%, stagnation pressure 0.7 bar; (d) DL-valine ethyl ester in He, 0.03%, stagnation pressure 0.7 bar.

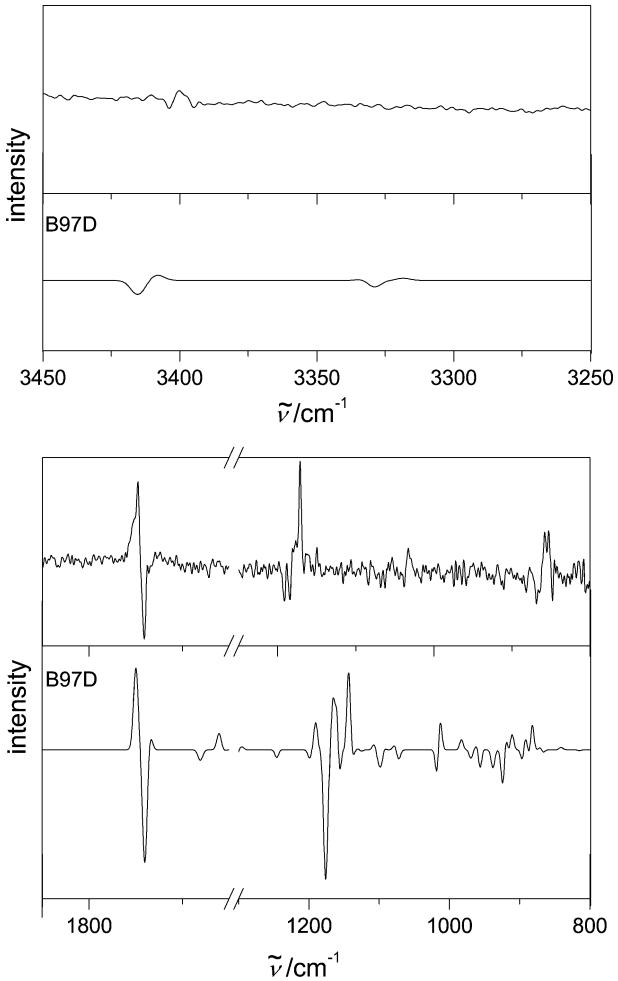

Fig. 16 Comparison of the experimental valine spectra obtained by subtraction with calculated difference spectra for the homochiral LL-8^{cc} dimer (downward peaks) and the heterochiral DL-8^{cc} dimer (upward peaks) at the B97D level for the NH (above) and carbonyl (below) stretching regions. The calculated spectra were simulated with a Gaussian line shape and a FWHM of 5 cm^{-1}. The intensity ratio between theory and experiment is fixed between the two spectral ranges.

along which the evolution of molecular properties can be followed. Several of these trends are documented in the ESI†, some of them shall be highlighted here:

The bifurcation trend (Table S6, ESI†) may be most important for the present work. In glycine, the NH_2 group forms two equivalent weak hydrogen bonds to the carbonyl group. In alanine the symmetry is slightly broken and in valine the torsion angles deviate by up to 19° and 49°, respectively. This changes the way in which the two functional groups interact and may also have effects on rovibrational coupling in this floppy system.

The carbonyl stretching wavenumber decreases with increasing residue size from 1764 to 1752 cm^{-1}. This is largely a through-bond electronic effect of the substituents. The NH stretching vibrations decrease from glycine to alanine and split in the case of valine due to rotational isomerism of the isopropyl group. The most striking experimental observation is the intensity increase of the antisymmetric stretching mode in both the IR and the Raman spectra upon cooling. It can be inferred from a comparison to robust CH stretching modes and amounts to about 25, <10, and 1 for glycine, alanine and valine in the Raman spectra and to about 7, <10, and 3 in the IR spectra, respectively. For the symmetric stretching mode the trend is much less pronounced. This effect is not easy to rationalize on the basis of *ab initio* calculations within the double-harmonic approximation (linear restoring force and linear dipole change with normal mode displacement) nor on the basis of intensity studies along large amplitude coordinates (see Fig. S3–S6, ESI†). However, it is likely to be connected to the conformational dynamics of the NH_2 group in the vicinity of a C=O group, as reference experiments for the C=O-deficient analogue show.

The electronic (D_e) and zero-point-corrected (D_0) dissociation energies of the most stable dimers (all except for DL-valine of the 8^{cc} type with isolated N–H···O=C bonds and a sandwich-like character) are instructive (Table S9, ESI†). Most of the driving force for aggregation is seen to arise from dispersion-driven folding interactions. Increasing residues lead to steadily increasing interaction energies in particular at the MP2 level. The trend is probably overestimated due to basis set superposition effects but a binding energy per monomer of ~20 kJ mol^{-1} may be estimated. The DL combination for valine allows for an additional twist with extra binding energy

despite the realization of a less stable N–H···O–C contact. This underscores the significance of interactions beyond local hydrogen bonding in amino acid esters.

4 Conclusions

It is not so surprising that vibrations with weak oscillator strength can show large intensity effects in the IR. However, the Raman cross section of terminal NH_2 groups is quite formidable and still there are enormous temperature variations observed in the monomer spectra. In summary, there are two challenges for an anharmonic theory of the NH-stretching dynamics of amino acid esters:

(i) Why is the antisymmetric NH-stretching intensity in the monomers so temperature dependent? Agreement with theory is only satisfactory at low temperatures or when the hydrogen bond bifurcation is removed by bulky substituents.

(ii) Why are the cluster NH-bands nearly invisible in the IR spectra? Inspection of the C=O- stretching range and the Raman spectra leaves no doubt that clustering is extensive under appropriate conditions but seems to avoid cooperative arrangements.

Furthermore, it was shown that B3LYP and B97D levels are unable to describe the spectral effects upon clustering, by predicting the wrong structures or wrong frequency shifts. At the harmonic MP2 level only the weak IR intensity of NH stretching transitions in dimers is poorly described. In addition to identifying these theoretical challenges, which invite future high level studies,[35,45] the present work allows for a few clearcut experimental conclusions:

(iii) Esters of amino acids can be prepared in a single conformation with respect to the weakly attractive $NH_2\cdots O{=}C$ arrangement.

(iv) Rearrangement to intermolecular $NH_2\cdots O{=}C$ hydrogen bonds upon aggregation leads to very small vibrational red-shifts of the involved NH_2-groups.

(v) If the amino acid residue is bulky enough such as in valine, chirality recognition in dimers can lead to differences in hydrogen bond topology.

It is not clear whether hydrogen bonding in amino acid esters should be classified as weak. Intramolecularly, it certainly is. On the other hand, the cohesion energy between two molecules is quite substantial and almost comparable to that of carboxylic acid dimers.[50] However, most of it seems to be of dispersive and electrostatic nature far from the hydrogen bond centers and the associated distortions of the intermolecular hydrogen bonds may contribute to their weak IR signature in terms of small wavenumber shifts and almost negligible intensity. We hope that our experimental work will trigger a high level theoretical analysis of the intensity anomalies in the monomers and clusters of these model compounds. High resolution IR spectroscopy may also contribute to the elucidation of the monomer intensity anomaly.

Acknowledgements

Extensive support by the research training group GRK 782 (www.pcgg.de) is gratefully acknowledged. The project has further profited from DFG funding (Su121/2) for the Raman jet spectrometer and from support by the Fonds der Chemischen Industrie.

References

1 A. G. Császár and A. Perczel, *Ab initio* characterization of building units in peptides and proteins, *Prog. Biophys. Mol. Biol.*, 1999, **71**, 243–309.
2 R. Linder, M. Nispel, T. Häber and K. Kleinermanns, Gas-phase FT-IR-spectra of natural amino acids, *Chem. Phys. Lett.*, 2005, **409**, 260–264.
3 R. Linder, K. Seefeld, A. Vavra and K. Kleinermanns, Gas-phase Infrared Spectra of Nonaromatic Amino Acids, *Chem. Phys. Lett.*, 2008, **453**, 1–6.
4 S. Blanco, A. Lesarri, J. C. López and J. L. Alonso, The Gas-phase Structure of Alanine, *J. Am. Chem. Soc.*, 2004, **126**, 11675–11683.
5 A. Lesarri, E. J. Cocinero, J. C. Lopez and J. L. Alonso, The Shape of Neutral Valine, *Angew. Chem., Int. Ed.*, 2004, **43**, 605–610.
6 R. M. Balabin, Conformational Equilibrium in Glycine: Experimental Jet-Cooled Raman Spectrum, *J. Phys. Chem. Lett.*, 2010, **1**, 20–23.
7 S. G. Stepanian, I. D. Reva, E. D. Radchenko and L. Adamowicz, Conformational Behavior of α-Alanine. Matrix-Isolation Infrared and Theoretical DFT and *ab initio* Study, *J. Phys. Chem. A*, 1998, **102**, 4623–4629.
8 S. G. Stepanian, I. D. Reva, E. D. Radchenko and L. Adamowicz, Combined Matrix-Isolation Infrared and Theoretical DFT and *ab initio* Study of the Nonionized Valine Conformers, *J. Phys. Chem. A*, 1999, **103**, 4404–4412.
9 R. Ramaekers, J. Pajak, M. Rospenk and G. Maes, Matrix-Isolation FTIR Spectroscopic Study and Theoretical DFT(B3LYP)/6-31++G** Calculations of the Vibrational and Conformational Properties of Tyrosine, *Spectrochim. Acta, Part A*, 2005, **61**, 1347–1356.
10 A. Kaczor, I. D. Reva, L. M. Proniewicz and R. Fausto, Importance of Entropy in the Conformational Equilibrium of Phenylalanine: Matrix-Isolation Infrared Spectroscopy and Density Functional Theory Study, *J. Phys. Chem. A*, 2006, **110**, 2369–2379.
11 C. Espinoza, J. Szczepanski, M. Vala and N. C. Polfer, Glycine and Its Hydrated Complexes: A Matrix Isolation Infrared Study, *J. Phys. Chem. A*, 2010, **114**, 5919–5927.
12 R. Schweitzer-Stenner, T. Measey, L. Kakalis, F. Jordan, S. Pizzanelli, C. Forte and K. Griebenow, Conformations of Alanine-Based Peptides in Water Probed by FTIR, Raman, Circular Dichroism, Electronic Circular Dichroism and NMR Spectroscopy, *Biochemistry*, 2007, **46**, 1587–1596.
13 G. D. Chumanov, R. G. Efremov and I. R. Nabiev, Surface-Enhanced Raman Spectroscopy of Biomolecules Part I-Water-Soluble Proteins, Dipeptides and Amino Acids, *J. Raman Spectrosc.*, 1990, **21**, 43–48.
14 M. Gerhards and C. Unterberg, Structures of the protected amino acid Ac–Phe–OMe and its dimer: A beta-sheet model system in the gas phase, *Phys. Chem. Chem. Phys.*, 2002, **4**, 1760–1765.
15 S. M. Bachrach, Microsolvation of Glycine: A DFT Study, *J. Phys. Chem. A*, 2008, **112**, 3722–3730.
16 J. T. O'Brien, J. S. Prell, J. D. Steill, J. Oomens and E. R. Williams, Changes in Binding Motif of Protonated Heterodimers Containing Valine and Amines Investigated Using IRMPD Spectroscopy between 800 and 3700 cm^{-1} and Theory, *J. Am. Chem. Soc.*, 2009, **131**, 3905–3912.
17 S. Hesse and M. A. Suhm, Conformation and Aggregation of Proline Esters and Their Aromatic Homologs: Pyramidal *vs.* Planar RR′N–H in Hydrogen Bonds, *Z. Phys. Chem.*, 2009, **223**, 579–604.
18 Y. D. Park, T. R. Rizzo, L. A. Petanu and D. H. Levy, Electronic Spectroscopy of Trytophan analogs in supersonic jets: 3-Indole acetic acid, 3-indole propionic acid, tryptamine and *N*-acetyl tryptophan ethyl ester, *J. Chem. Phys.*, 1986, **84**, 6539–6549.
19 J. A. Stearns, S. R. Mercier, C. Seaiby, M. Guidi, O. V. Boyarkin and T. R. Rizzo, Conformation-Specific Spectroscopy and Photodissociation of Cold Protonated Tyrosine andPhenylalanine, *J. Am. Chem. Soc.*, 2007, **129**, 11814–11820.

20 P. Carcabal, R. T. Kroemer, L. C. Snoek, J. P. Simons, J. M. Bakker, I. Compagnon, G. Meijer and G. von Helden, Hydrated Complexes of Tryptophan: Ion Dip Infrared Spectroscopy in the molecular Fingerprint region, 100–2000 cm^{-1}, *Phys. Chem. Chem. Phys.*, 2004, **6**, 4546–4552.

21 A. Kamariotis, O. V. Boyarkin, S. R. Mercier, R. D. Beck, M. F. Bush, E. R. Williams and T. R. Rizzo, Infrared Spectroscopy of Hydrated Amino Acids in the Gas Phase: Protonated and Lithiated Valine, *J. Am. Chem. Soc.*, 2005, **128**, 905–916.

22 W. K. Mino, K. Gulyuz, D. Wang, C. N. Stedwell and N. C. Polfer, Gas-Phase Structure and Dissociation Chemistry of Protonated Tryptophan Elucidated by Infrared Multiple-Photon Dissociation Spectroscopy, *J. Phys. Chem. Lett.*, 2011, **2**, 299–304.

23 S. Hesse, T. N. Wassermann and M. A. Suhm, Brightening and locking a weak and floppy N–H chromophore: The case of pyrrolidine, *J. Phys. Chem. A*, 2010, **114**, 10492–10499.

24 Y. S. Lee, H. W. Kim and S. S. Park, The Role of α-Amino Group of the N-terminal Serine of β Subunit for Enzyme Catalysis and Autoproteolytic Activation of Glutaryl 7-Aminocephalosporanic Acid Acylase, *J. Biol. Chem.*, 2000, **275**, 39200–39206.

25 I. V. Alabugin, M. Manoharan, S. Peabody and F. Weinhold, Electronic Basis of Improper Hydrogen Bonding: A Subtle Balance of Hyperconjugation and Rehybridization, *J. Am. Chem. Soc.*, 2003, **125**, 5973–5987.

26 J. Joseph and E. D. Jemmis, Red-, Blue-, or No-Shift in Hydrogen Bonds: A Unified Explanation, *J. Am. Chem. Soc.*, 2007, **129**, 4620–4632.

27 N. Borho, M. A. Suhm, K. Le Barbu-Debus and A. Zehnacker, Intra- *vs.* Intermolecular Hydrogen Bonding: Dimers of alpha-Hydroxyesters with Methanol, *Phys. Chem. Chem. Phys.*, 2006, **8**, 4449–4460.

28 P. Zielke and M. A. Suhm, Concerted proton motion in hydrogen-bonded trimers: a spontaneous scattering Raman perspective, *Phys. Chem. Chem. Phys.*, 2006, **8**, 2826–2830.

29 J. J. Lee, S. Höfener, W. Klopper, T. N. Wassermann and M. A. Suhm, Origin of the Argon nanocoating shift in the OH-Stretching fundamental of *n*-propanol: a combined experimental and quantum chemical study, *J. Phys. Chem. C*, 2009, **113**, 10929–10938.

30 T. N. Wassermann and M. A. Suhm, Ethanol monomers and dimers revisited: A Raman study of conformational preferences and argon nanocoating effects, *J. Phys. Chem. A*, 2010, **114**, 8223–8233.

31 M. J. Frisch, G. W. Trucks, H. B. Schlegel, G. E. Scuseria, M. A. Robb, J. R. Cheeseman, G. Scalmani, V. Barone, B. Mennucci, G. A. Petersson, H. Nakatsuji, M. Caricato, X. Li, H. P. Hratchian, A. F. Izmaylov, J. Bloino, G. Zheng, J. L. Sonnenberg, M. Hada, M. Ehara, K. Toyota, R. Fukuda, J. Hasegawa, M. Ishida, T. Nakajima, Y. Honda, O. Kitao, H. Nakai, T. Vreven, J. J. A. Montgomery, J. E. Peralta, F. Ogliaro, M. Bearpark, J. J. Heyd, E. Brothers, K. N. Kudin, V. N. Staroverov, R. Kobayashi, J. Normand, K. Raghavachari, A. Rendell, J. C. Burant, S. S. Iyengar, J. Tomas, M. Cossi, N. Rega, J. M. Millam, M. Klene, J. E. Knox, J. B. Cross, V. Bakken, C. Adamo, J. Jaramillo, R. Gomperts, R. E. Stratmann, O. Yazyev, A. J. Austin, R. Cammi, C. Pomelli, J. W. Ochterski, R. L. Martin, K. Morokuma, V. G. Zakrzewski, G. A. Voth, P. Salvador, J. J. Dannenberg, S. Dapprich, A. D. Daniels, O. Farkas, J. B. Foresman, J. V. Ortiz, J. Cioslowski and D. J. Fox, *Gaussian 09, Revision A.02*, 2009.

32 L. Schäfer, C. V. Alsenoy, J. N. Scarsdale, V. J. Klimkowski and J. D. Ewbank, *Ab initio* Studies of Structural Features not Easily Amenable to Experiment. 18. Conformational Analysis and Molecular Structure of Glycine Methyl Ester, *J. Comput. Chem.*, 1981, **2**, 410–413.

33 W. Caminati and R. Cervekkati, Bifurcated Hydrogen Bond and Large Amplitude Vibrations in Glycine Methyl Ester, *J. Am. Chem. Soc.*, 1982, **104**, 4748–4752.

34 R. M. Balabin, Conformational equilibrium in glycine: Focal-point analysis and *ab initio* limit, *Chem. Phys. Lett.*, 2009, **479**, 195–200.

35 V. Kasalová, W. D. Allen, H. F. Schaefer, III, E. Czinki and A. G. Császár, Molecular structures of the two most stable conformers of free glycine, *J. Comput. Chem.*, 2007, **28**, 1373–1383.

36 P. D. Godfrey, R. D. Brown and F. M. Rodgers, The missing conformers of glycine and alanine: relaxation in seeded supersonic jets, *J. Mol. Struct.*, 1996, **376**, 65–81.

37 I. Hünig and K. Kleinermanns, Conformers of the Peptides Glycine–Tryptophan, Tryptophan–Glycine and Tryptophan–Glycine–Glycine as Revealed by Double Resonance Laser Spectroscopy, *Phys. Chem. Chem. Phys.*, 2004, **6**, 2650–2658.

38 A. P. Gray and R. C. Lord, Rotation-Vibration Spectra of Methylamine and its Deuterium Derivatives, *J. Chem. Phys.*, 1957, **26**, 690–705.

39 Y. Hamada, N. Tanaka, Y. Sugawara, A. Y. Hirakawa, M. Tsuboi, S. Kato and K. Morokuma, Force Field in the Methylamine Molecule from *ab initio* MLO Calculation, *J. Mol. Spectrosc.*, 1982, **96**, 313–330.

40 C. J. Purnell, A. J. Barnes, S. Suzuki, D. F. Ball and W. J. Orville-Thomas, Infrared and Raman Matrix Isolation studies of Methylamine, *Chem. Phys.*, 1976, **12**, 77–87.

41 U. Merker, H. K. Srivatava, A. Callegari, K. K. Lehmann and G. Scoles, Eigenstate resolved infrared and millimeter-wave-infrared double resonance spectroscopy of methylamine in the N–H stretch first overtone region, *Phys. Chem. Chem. Phys.*, 1999, **1**, 2427–2433.

42 F. Huisken, O. Werhahn, A. Y. Ivanov and S. A. Krasnokutski, The O–H stretching vibrations of glycine trapped in rare gas matrices and helium clusters, *J. Chem. Phys.*, 1999, **111**, 2978–2984.

43 W. Caminati, 2-Methoxyethylamine: Detection of a second conformer by microwave spectroscopy, *J. Mol. Spectrosc.*, 1987, **121**, 61–68.

44 J. D. Ewbank, V. J. Klimkowski, K. Siam and L. Schäfer, Conformational Analysis of the Methyl Ester of Alanine by Gas Electron Diffraction and *ab initio* Geometry Optimization, *J. Mol. Struct.*, 1987, **160**, 275–285.

45 H. M. Jaeger, H. F. Schaefer, III, J. Demaison, A. G. Császár and W. D. Allen, Lowest-Lying Conformers of Alanine: Pushing Theory to Ascertain Precise Energetics and Semiexperimental R_e Structures, *J. Chem. Theory Comput.*, 2010, **6**, 3066–3078.

46 B. Lambie, R. Ramaekers and G. Maes, On the Contribution of Intramolecular H-bonding Entropy to the Conformational Stability of Alanine Conformations, *Spectrochim. Acta, Part A*, 2003, **59**, 1387–1397.

47 S. Dokmaisrijan, V. S. Lee and P. Nimmanpipug, The gas phase conformers and vibrational spectra of valine, leucine and isoleucine: An *ab initio* study, *THEOCHEM*, 2010, **953**, 28–38.

48 A. Zehnacker and M. A. Suhm, Chirality recognition between neutral molecules in the gas phase, *Angew. Chem., Int. Ed.*, 2008, **47**, 6970–6992.

49 N. Borho and M. A. Suhm, Glycidol dimer: anatomy of a molecular handshake, *Phys. Chem. Chem. Phys.*, 2002, **4**, 2721–2732.

50 Z. Xue and M. A. Suhm, Adding more weight to a molecular recognition unit: the low-frequency modes of carboxylic acid dimers, *Mol. Phys.*, 2010, **108**, 2279–2288.

